JPE 9-5-12

Direct Power Control of a DFIG in Wind Turbines to Improve Dynamic Responses

Sung-Tak Jou*, Sol-Bin Lee*, Yong-Bae Park*, and Kyo-Beum Lee†

†*Division of Electrical and Computer Engineering, Ajou University, Suwon, Korea

ABSTRACT

This paper presents an implementation of a direct active and reactive power control for a doubly fed induction generator (DFIG), which is applied to a wind generation system as an alternative to the classical field-oriented control (FOC). The FOC has a complex control structure that consists of a current controller, a power controller and frame transformations. The performance of the FOC depends highly on parameter variations of the rotor and stator resistances and the inductances. The proposed direct power control (DPC) method produces a fast and robust power response without the need of complex structure and algorithms. One drawback, however, is its high power ripple during a steady state. In this paper, active and reactive power controllers and space-vector modulation (SVM) are combined to replace hysteresis controllers used in the original DPC drive, resulting in a fixed switching frequency of the power converter. Simulation results with the FOC and DPC for a 3kW DFIG are given and discussed, and the experimental results of a test involving identical machines are presented to illustrate the feasibility of the proposed control strategy.

Keywords: Direct power control, Doubly fed induction generator, Space-vector modulation, Fixed switching frequency

1. Introduction

The doubly fed induction generator (DFIG) applied to wind generation systems has been of interest due to its significant market potential. This system allows variable speed operation over a large but restricted range. A DFIG consists of a wound rotor induction generator (WRIG) with the stator windings directly connected to a three-phase power grid and with the rotor windings mounted to a bidirectional back-to-back IGBT frequency converter[1-4]. A schematic diagram of a variable-speed wind turbine system with a DFIG is shown in Fig. 1.

The power converter consists of a rotor-side converter and a grid-side converter in which the rotor-side converter controls the active and reactive power and the grid-side converter controls the DC-link voltage and ensures operation of the converter at a unity power factor [5]. Control of a DFIG is traditionally achieved through control of the components of the voltage vector in a field-oriented control (FOC), which is achieved by a rotor current controller[6-9]. One main drawback of this system is that its performance depends greatly on accurate machine parameters pertaining to the stator, rotor resistances,

Manuscript received July 26, 2008; revised July 30, 2009.
†Corresponding Author: kyl@ajou.ac.kr
Tel: +82-31-219-2376, Fax: +82-31-212-9531, Ajou Univ.
*Division of Electrical and Comp. Eng., Ajou Univ.

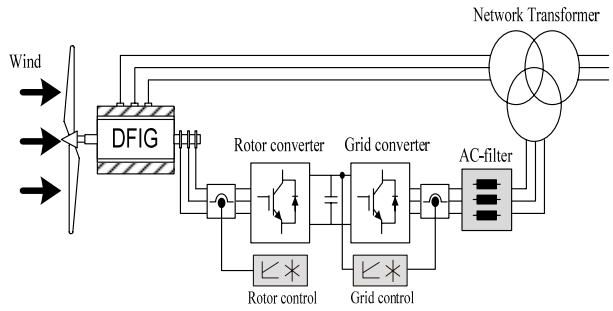

Fig. 1. Schematic diagram of a variable-speed wind turbine system with a DFIG.

and inductances.

Thus, the performance degrades when the actual machine parameters depart from the values used in the control system. Direct power control (DPC) abandons the rotor current control philosophy, which is the characteristic of FOC. Also, DPC achieves bang-bang active and reactive power control by the modulation of the rotor voltage in accordance with the active and reactive power errors. DPC is characterized by its fast dynamic response, simple structure and robust response against parameter variations. It does not utilize a rotor current controller and SVM[10-11]. One drawback of a basic DPC is that it displays large current, active and reactive power ripple, resulting in vibration and acoustic noise. Another drawback of DPC is a converter switching frequency variation that significantly complicates the design of the power circuit. In order to obtain a smooth operation and at a fixed switching frequency, direct power control is combined with a SVM strategy based on the principles of the DPC method.

This paper presents a new direct active and reactive power control based on SVM for a DFIG-based wind turbine system. The control strategy directly calculates the reference rotor control voltage with each switching period using the estimated stator flux along with the calculated active and reactive powers and their errors. Simulation results for a 3 kW are presented and discussed, and experimental results for a 3 kW demonstrate the performance of the proposed control strategy.

2. Modeling of the DFIG

The DFIG is a wound rotor induction generator in

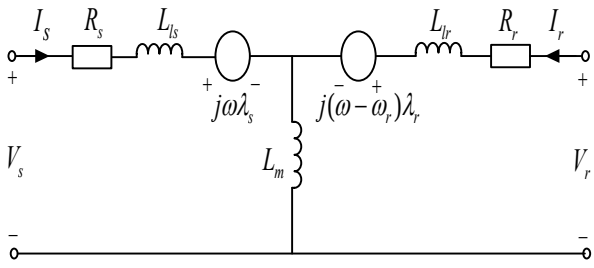

Fig. 2. An equivalent circuit in an arbitrary reference frame.

which the rotor circuit is connected to the grid through two back-to-back converters with a common DC link capacitor bank. The ability to subtract power from and supply power to the rotor makes it possible to operate the DFIG at sub-synchronous or super-synchronous speeds while maintaining a constant voltage and frequency on the stator [12-14]. The d-q model in the arbitrary reference frame is expressed as follows:

$$V_s = R_s I_s + \frac{d\lambda_s}{dt} + j\omega\lambda_s \tag{1}$$

$$V_r = R_r I_r + \frac{d\lambda_r}{dt} + j(\omega-\omega_r)\lambda_r \tag{2}$$

$$\begin{aligned} &\lambda_s = \lambda_{ds} + j\lambda_{qs}, \quad \lambda_r = \lambda_{dr} + j\lambda_{qr} \\ &\lambda_{ds} = L_s I_{ds} + L_m I_{dr}, \quad \lambda_{qs} = L_s I_{qs} + L_m I_{qr} \\ &\lambda_{dr} = L_r I_{dr} + L_m I_{ds}, \quad \lambda_{qr} = L_r I_{qr} + L_m I_{qs} \end{aligned} \tag{3}$$

where I_{ds}, I_{qs}, I_{dr}, I_{qr} are the currents and the fluxes of the stator and rotor in d and q-axes, R_s and R_r are the resistances of the stator and rotor windings, and ω_r is the rotor speed. An equivalent circuit is set up by means of the voltage and flux equations of an arbitrary reference frame, as shown in Fig. 2.

The rotor-side converter is controlled in a synchronously rotating dq-axis frame, with the d-axis oriented along the stator flux vector position. In this approach, decoupled control between the stator active and reactive powers is obtained. The influence of the stator resistance can be neglected and the stator flux can be held constant as the stator is connected to the grid. For such a reference frame selection, the DFIG model can be derived as

$$V_{ds} = 0, \; V_{qs} = \omega_s \lambda_{ds} \tag{4}$$

$$V_{dr} = (R_r + R_s \frac{L_m^2}{L_s^2}) I_{dr} + \sigma L_r \frac{dI_{dr}}{dt} - \omega_{sl} \sigma L_r I_{qr}$$
$$V_{qr} = (R_r + R_s \frac{L_m^2}{L_s^2}) I_{qr} + \sigma L_r \frac{dI_{qr}}{dt} + \omega_{sl}(L_{mm} I_{ms} + \sigma L_r I_{dr}) \quad (5)$$

$$\lambda_{ds} = L_m I_{ms} = L_s I_{ds} + L_m I_{dr}$$
$$\lambda_{qs} = L_s I_{qs} + L_m I_{qr} = 0 \quad (6)$$

$$\lambda_{dr} = \frac{L_m^2}{L_s} I_{ms} + \sigma L_r I_{dr}, \quad \lambda_{qr} = \sigma L_r I_{qr} \quad (7)$$

where $\sigma = 1 - L_m^2 / L_s L_r$, $L_{mm} = L_m^2 / L_s$, $\omega_{sl} = \omega_s - \omega_r$ is the slip frequency, ω_s is the electrical angular velocity of the stator, and I_{ms} is the magnetizing current of the generator.

The DFIG stator active and reactive powers are computed as follows:

$$P_s = \frac{3}{2}(V_{ds} I_{ds} + V_{qs} I_{qs}) = -\frac{3}{2} \frac{L_m}{L_s} V_{qs} I_{qr}$$
$$Q_s = \frac{3}{2}(V_{qs} I_{ds} - V_{ds} I_{qs}) = \frac{3}{2} V_{qs} (\frac{L_m}{L_s} I_{dr} - \frac{V_{qs}}{\omega_s L_s}). \quad (8)$$

Due to the constant stator voltage, the stator active and reactive powers are controlled by means of I_{qr} and I_{dr}, respectively [15].

3. Maximum Power Point Tracking(MPPT) Strategy

The output power of a turbine is given by the following equation.

$$P_t = \frac{1}{2} A \rho C_{P\_\max} \left(\frac{R}{\lambda_{opt}} \right)^3 \omega_t^3 \quad (9)$$

where A is cross-sectional area[m2]; ρ is the air density [kg/m2]; C_{p_max} is the power coefficient; R is the radius of turbine [m], and ωt is the turbine speed [rad/s]. Since the C_{p_max} is always maintained at maximum value, the power output of the turbine is controlled by the rotor speed. From (9), the generator torque can be calculated as

$$T_g = \frac{1}{2} A \rho C_{P\_\max} \left(\frac{R}{\lambda_{opt}} \right)^3 \omega_t^2. \quad (10)$$

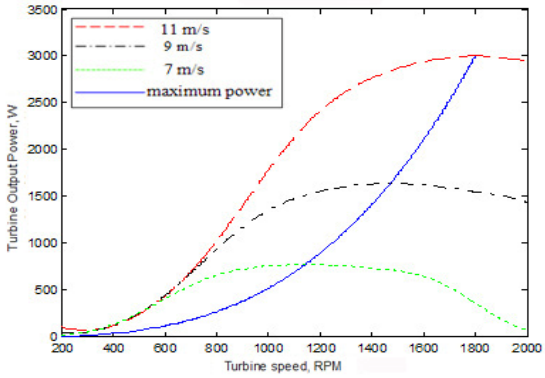

Fig. 3. Turbine Power as a function of turbine speed for different wind velocities.

Converted to electrical energy in generator torque T_e is as follows

$$T_e = T_t - B\omega_t \quad (11)$$

where B is friction coefficient that contains all of friction elements that exist between a blade and a generator.

The typical power-speed characteristics of a wind turbine at different wind speeds, having a fixed pitch angle, are shown in Fig.3. It can be seen that the turbine speeds for maximum output power are different for different wind speeds [16].

4. Proposed Direct Power Control for the DFIG

In the proposed control strategy, the d-axis of the synchronous frame is fixed to the stator flux. As the stator is directly connected to the grid, and since the influence of the stator resistance can be neglected, the stator flux can be held constant. From (1), for a synchronous frame (the stator flux speed), the stator voltage vector is given as

$$V_s^{\omega} = V_{qs} = \omega_s \lambda_{ds}. \quad (12)$$

Based on (3), the stator current is expressed by

$$I_s^{\omega} = \frac{L_r \lambda_s^{\omega} - L_m \lambda_r^{\omega}}{L_s L_r - L_m} = \frac{\lambda_s^{\omega}}{\sigma L_s} - \frac{L_m \lambda_r^{\omega}}{\sigma L_s L_r}. \quad (13)$$

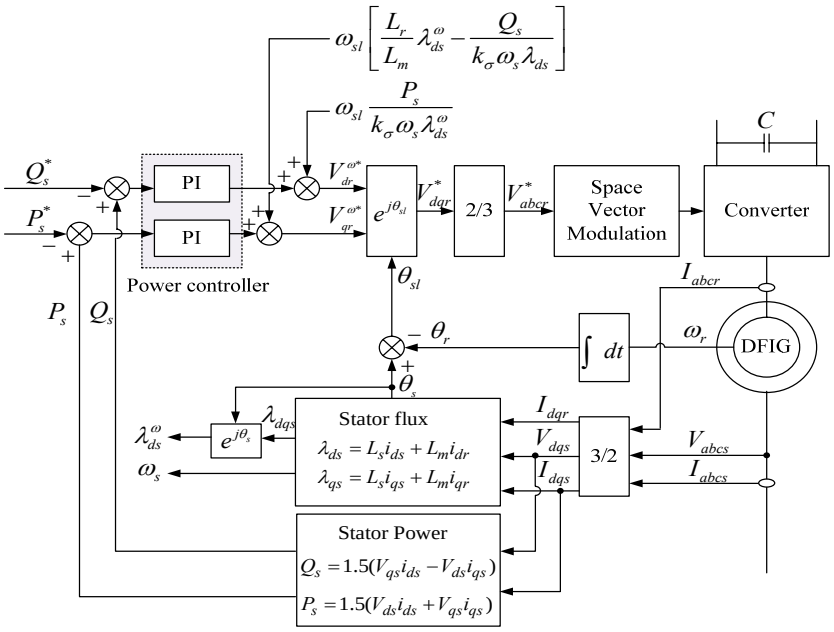

Fig. 4. Schematic diagram of the proposed DPC for a DFIG system.

Using (8) and (10), the stator active and reactive power inputs from the network can be calculated as

$$\begin{aligned} P_s &= -k_\sigma \omega_s \lambda_{ds}^{\omega} \lambda_{qr}^{\omega} \\ Q_s &= k_\sigma \omega_s \lambda_{ds}^{\omega} \left(\frac{L_r}{L_m} \lambda_{ds}^{\omega} - \lambda_{dr}^{\omega}\right) \end{aligned} \tag{14}$$

where $k_\sigma = 1.5 L_m / (\sigma L_s L_r)$.

As the stator flux remains constant, according to (14) the active and reactive power changes over a constant period of Ts are given by

$$\begin{aligned} \Delta P_s &= -k_\sigma \omega_s \lambda_{ds}^{\omega} \Delta \lambda_{qr}^{\omega} \\ \Delta Q_s &= -k_\sigma \omega_s \lambda_{ds}^{\omega} \Delta \lambda_{dr}^{\omega}. \end{aligned} \tag{15}$$

In the synchronous d-q reference frame, the rotor voltage is given by

$$V_r^{\omega} = R_r I_r^{\omega} + \frac{d\lambda_r^{\omega}}{dt} + j\omega_{sl} \lambda_r^{\omega}. \tag{16}$$

Combining (14), (15) and (16) and neglecting the rotor resistance, the rotor voltage required to eliminate the power errors in the d-q reference frame is calculated as

$$\begin{aligned} V_{dr}^{\omega} &= (K_{PQ} + K_{IQ}/s)(Q_s - Q_s^*) + \omega_{sl} \frac{P_s}{k_\sigma \omega_s \lambda_{ds}^{\omega}} \\ V_{qr}^{\omega} &= (KP + K_{IP}/s)(P_s - P_s^*) + \omega_{sl} \left(\frac{L_r}{L_m} \lambda_{ds}^{\omega} - \frac{Q_s}{k_\sigma \omega_s \lambda_{ds}^{\omega}}\right). \end{aligned} \tag{17}$$

The first terms on the right hand side reduce the number of power errors while the second terms offset the rotor slip that results from the different rotating speeds of the stator and rotor fluxes. As it can be seen, the calculations require only simple multiplications and avoid complicated mathematics.

A schematic diagram of the proposed DPC for a DFIG system is shown in Fig. 4. The controller contains two PI controllers, one for an active power and one for reactive power, as well as a SVM unit.

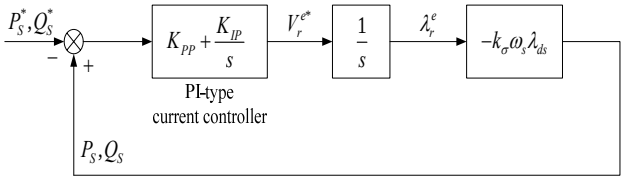

Fig. 5. Overall control system of the DPC.

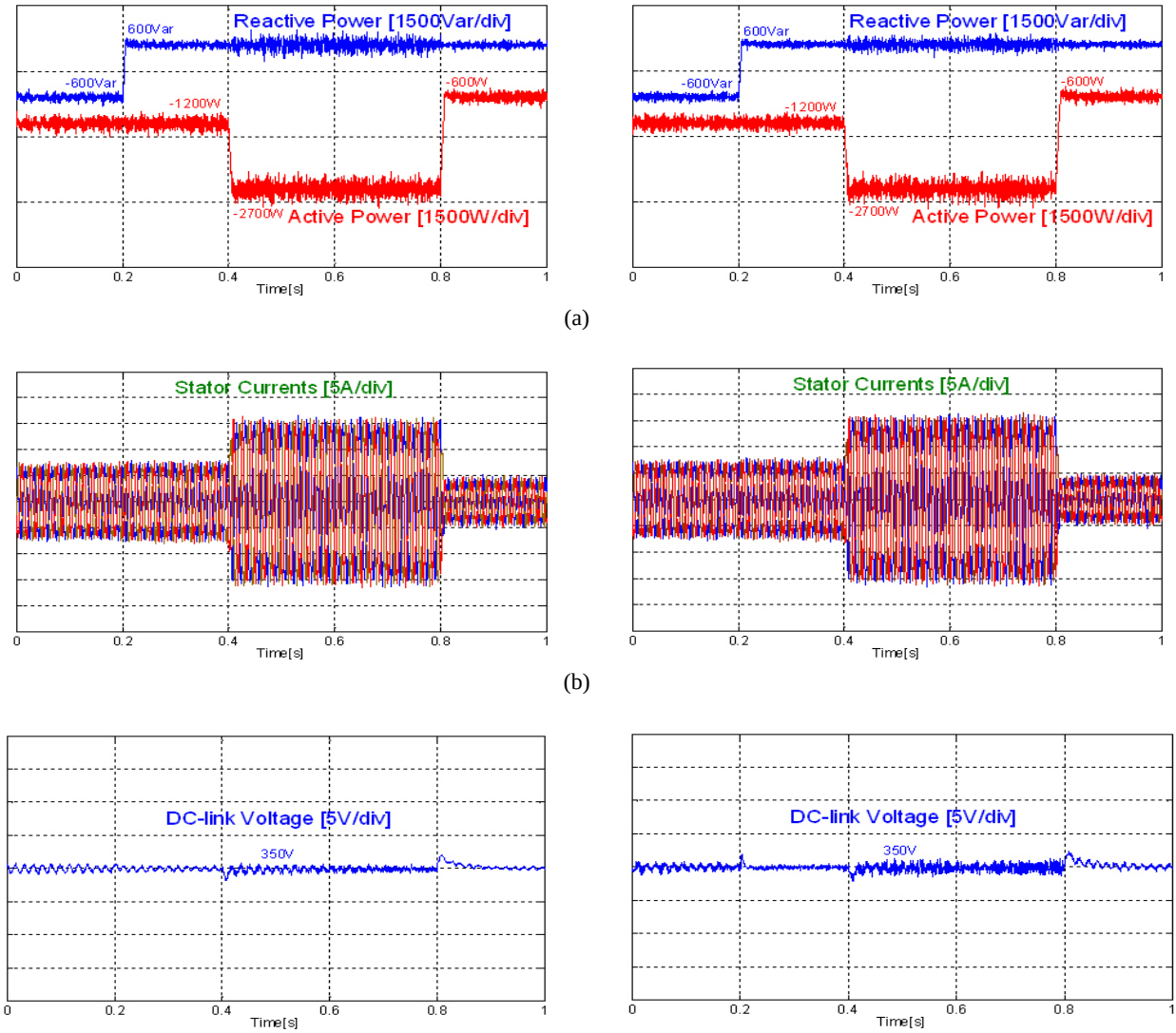

(A) With nominal L_m (B) With $0.5L_m$

Fig. 6. Simulation results of the power step responses (a), stator currents (b) and DC-link voltage (c) in the DPC drive.

The stator active and reactive powers can be calculated directly. The stator flux is estimated using the measured stator voltages and currents in the stationary reference. Considering (14), (16) and (17), a block diagram displays the dynamics existing between P_s and $V_{qr}{}^{\omega *}$ on the one hand, and between Q_s and $V_{dr}{}^{\omega *}$ on the other hand.

The overall control structure of a DPC is essentially constituted by one power controller. Fig. 5 shows that both dynamics are identical. Furthermore, this stator flux may be regarded as a constant disturbance whose effect on Q_s can be removed easily simply by closing the reactive power control-loop via a compensator that includes an integral action. It is fundamental to note that the error signals feeding the PI controller are computed by subtracting the set-point of the variable to be controlled, Q_s* or P_s*, from its actual value, Q_s or P_s, respectively. This is due to the fact that Q_s* and Q_s are strictly negative. As a result, both Q_s and P_s closed-loop dynamics can be represented by the following unique second-order transfer function:

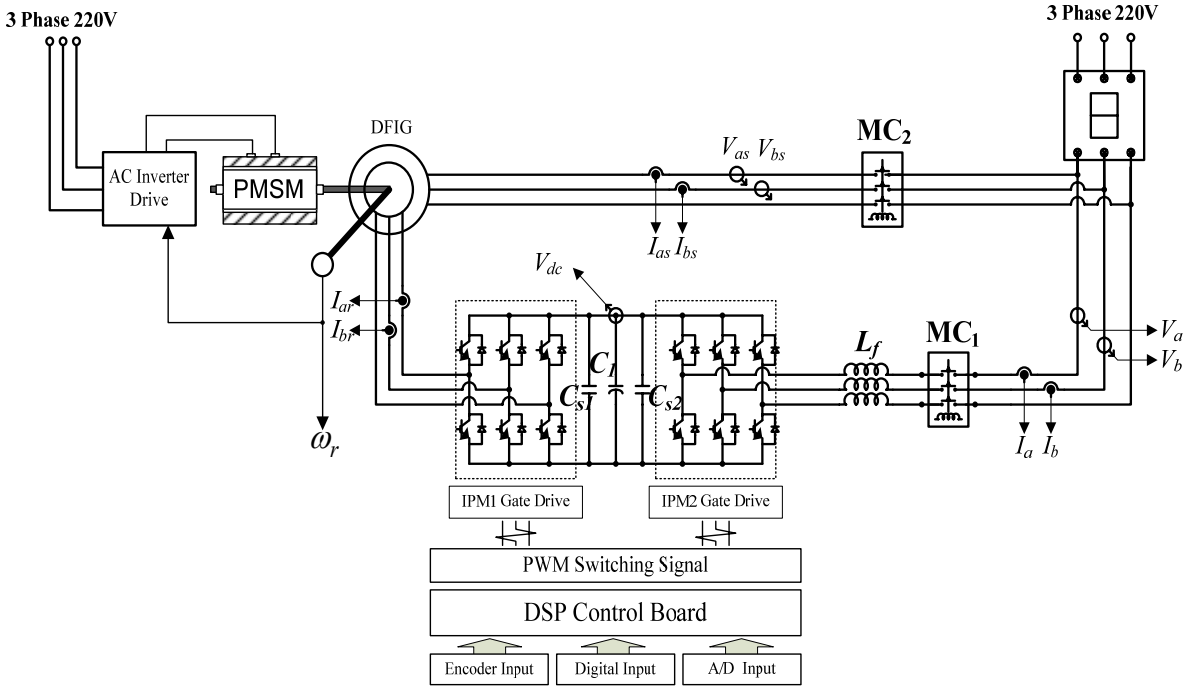

(a) Schematic diagram of the experimental setup

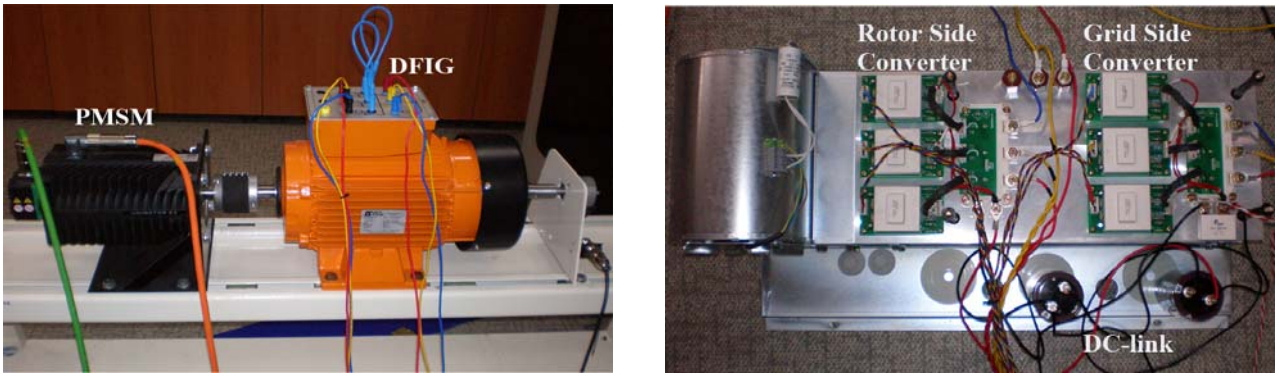

(b) Actual picture of the experimental setup

Fig. 7. Experimental setup of the DPC system.

$$\frac{P_s}{P_s^*}=\frac{Q_s}{Q_s^*}\approx\frac{K_{PP}k_\sigma\omega_s\lambda_{ds}^{\omega}(s+\frac{K_{IP}}{K_{PP}})}{s^2+K_{PP}k_\sigma\omega_s\lambda_{ds}^{\omega}s+K_{IP}k_\sigma\omega_s\lambda_{ds}^{\omega}}. \quad (18)$$

From the transfer function (18), the dynamics are mainly influenced by constant k_σ values that are determined via the stator and rotor leakage and the mutual inductance. Substituting the stator and rotor inductances (3), the parameter k_σ is rewritten as follows:

$$k_\sigma=\frac{3}{2}\frac{L_m}{L_sL_r-L_m^2}\approx\frac{3}{2}\frac{1}{L_{ls}+L_{sr}}. \quad (19)$$

Considering that the leakage path is mainly air, the variation of machine parameter has little impact on the power dynamics.

5. Simulation Results

A Simulation of the proposed control strategy for a

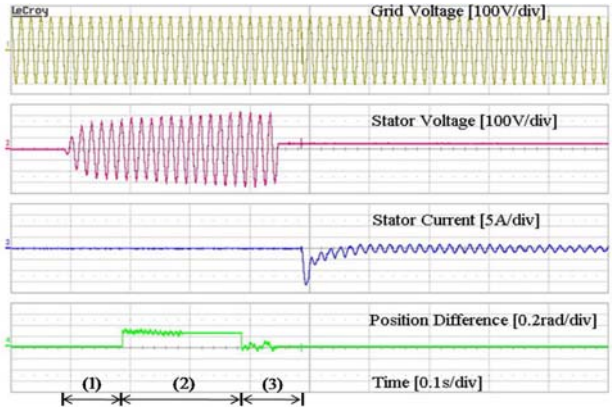

Fig. 8. Experimental results of the connection to the grid.

DFIG-based generation system was performed to show that the DPC drive is able to operate with fast dynamic response and robustness of the reactive and active power control in. The DPC strategy was simulated using a 3kW, 220V, 14.7A, 60Hz four-pole machine with the parameters R_s=0.667 Ω , R_r=0.625 Ω , L_s=67.3mH, L_r=67.3mH, and L_m=63.9mH. Fig. 6-(a) shows the power response of the DPC drive when the active and reactive powers are step-changed from -600Var to 600Var at steps of 0.2s and from -1200W to -2700W at steps of 0.4s, respectively ("-" refers to the generation of active power and to the absorption of reactive power). The DPC strategy has a faster dynamic response than the FOC strategy. A FOC drive is sensitive to the changes in the mutual inductance. Fig. 6-(A) and (B) show the simulation with the mutual inductance used in the controller having 0% and 50% errors, respectively. Fig. 6-(B) shows the robustness of the DPC drive. This does not depend on the variation of the mutual inductance and shows robust characteristics against parameter variations.

6. Experimental Results

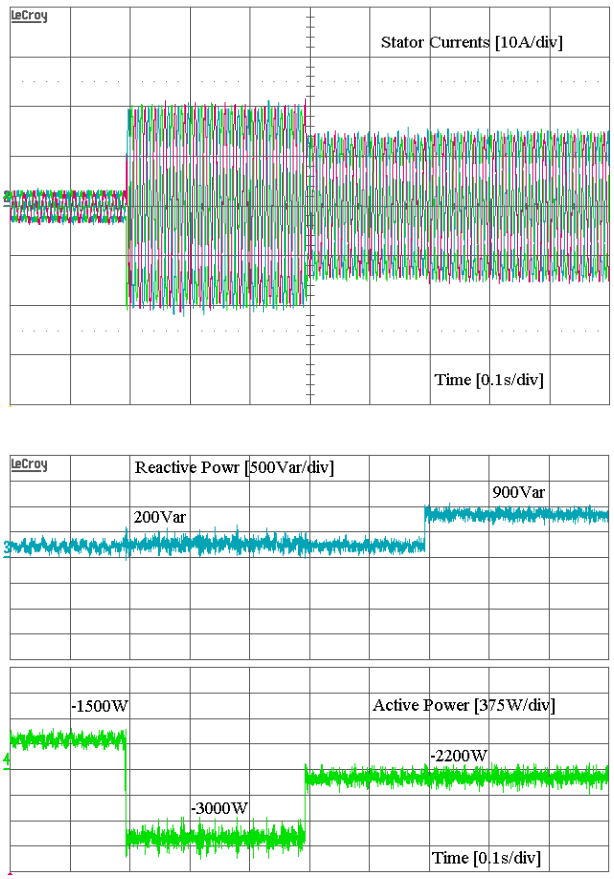

Fig. 9. Experimental results of the proposed DPC step responses.

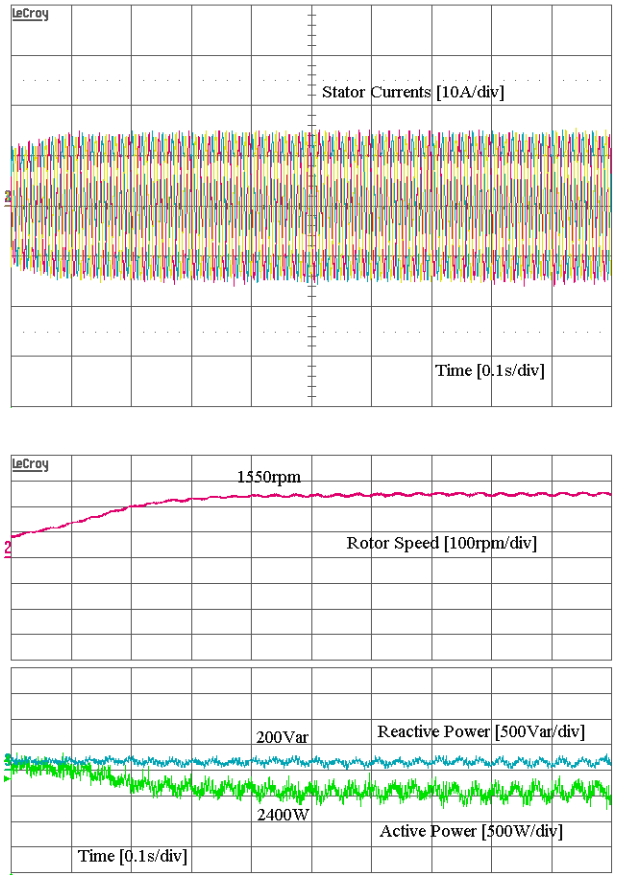

Fig. 10. Experimental results of a complete generation system.

The experimental setup of the DPC system is shown in Fig.7. The rated values and parameters of the DFIG are identical to those in the simulation. The generator is driven by 4.96kW and 220V of power at 3000rpm PMSM. The power electronic stages consist of two back-to-back converters using intelligent power modules (IPM).

The rotor-side voltage source PWM converter is inserted into the rotor winding and the grid-side voltage source PWM converter is connected to the stator winding via an AC filter. The converters are 3kW-rated IGBT bridges with a 2400μF DC-link capacitor. The sampling time is 100μs and the switching frequency is 5 kHz. The digital controller is based on a digital signal processor (TMS320VC33 DSP) and a 12-bit analogue-to-digital (A/D) converter, providing fast processing for floating-point calculations. Hall sensors are used in the current measurement, and the reference voltages are synthesized from the regulated DC-link voltage and SVM signals of the converters. The sampling time during the experiment was 100μs, and the rotor side converter switching time was 200μs. The dead time compensation was also included [5]. During the experiment, two processes were carried out before the stator winding was connected to the grid via a magnetic contactor (MC). First, at lower rotor speeds, the power generation from the DFIG is inadequate to supply to the grid. The magnetic contactor is activated when the rotor speed reaches a set rotor speed. Secondly, the stator winding is connected to the grid when the stator voltage, frequency and phase are aligned to the grid. Fig. 8 shows that the stator winding is connected to the grid within 0.4 s. In region 1 (see Fig. 8, 0.1sec-0.18sec), the magnetizing current is applied to the rotor. In region 2 (see Fig. 8, 0.18sec-0.38sec), the phase differences of grid voltages and stator voltages are calculated. In region 3 (see Fig. 8, 0.38sec-0.48sec), the magnitude and phase of the rotor current is, then, controlled so that the grid voltage and the stator voltage can be synchronized.

The DPC controller gains used are as follows: $K_{PQ} = 0.5$, $K_{IQ} = 500$, $K_{PP} = 0.5$, and $K_{IP} = 500$. To verify the proposed control strategy, an experimental investigation focused on the active and reactive power response and the stator current ripple was conducted. The active and reactive power references were step-changed from -3 kW to -2.2 kW at steps of 0.5 s and from -0.2 kVar to 0.9 kVar at steps of 0.7 s, respectively. In this process, no overshoot existed during the transient operation and the steady-state error was held constant. The effectiveness of the proposed DPC strategy is confirmed in Fig. 9. For the MPPT curve of a variable-speed wind turbine [16], tests of a complete generation system were carried out. The DFIG was set in power control. Given a rotor-speed measurement using an encoder, active power references were calculated from the MPPT curve and were imposed on the DFIG after compensating for power losses. Fig. 10 shows the experimental result when the rotor speed changes from 1480 to 1550 rpm. In Fig. 10, the generation system operated well and achieved the MPPT curve during variation of the rotor speed.

7. Conclusion

A direct power control method for DFIG drives was proposed to control the active and reactive powers directly without the need of the frame transformation and the current controller used in a FOC drive. This facilitated the robustness of the proposed method. Both the simulation and the experimental results demonstrate the validity of the DPC algorithm with a fixed switching frequency. Compared to a FOC drive, the proposed control strategy can provide fast dynamic responses under transient conditions and robust characteristics against parameter variations.

Acknowledgements

This work was supported by the Ajou University under Research Grant 20083770.

References

[1] T. Ackermann, *Wind Power in Power Systems*. John Wiley and Sons, 2005.

[2] B. M. Dehkordi, A. F. Payam, M. N. Hashemnia, and S. -K. Sul, "Design of an Adaptive Backstepping controller for Doubly-Fed Induction Machine Drives," *Journal of Power Electronics*, Vol. 9, no. 3, pp. 343-353, Mar. 2009.

[3] O. S. Ebrahim, P. K. Jain, and G. Nishith, "New Control Scheme for the Wind-Driven Doubly Fed Induction

Generator under Normal and Abnormal Grid Voltage Conditions," *Journal of Power Electronics*, Vol. 8, no. 1, pp. 10-22, Jan. 2008.

[4] G. –B. Chung, and J. –H. Choi, "Application of Fuzzy PI Control Algorithm as Stator Power Controller of Double-Fed Induction Machine in Wind Power Generation Systems," *Journal of Power Electronics*, Vol. 9, no. 1, pp. 109-116, Jan. 2008.

[5] I. Boldea, *Electric Drives*, Taylor & Francis, 2006.

[6] S. Arnalte, J. C. Burgos and J. L. R. Amenedo, "Direct Torque Control of a Doubly-Fed Induction Generator for Variable Speed Wind Turbines," *Electric Power Components and Systems*, Vol. 30, no. 1, pp. 199-216, Jan. 2002.

[7] K. P. Gokhale, D. W. Karraker, and S. J. Heikkila, "Controller for a Wound Rotor Slip Ring Induction Machine," *U. S. Patent*, no. US2003/0071596, Apr. 2003.

[8] K. -B. Lee, C. -H. Bae, and F. Blaabjerg, "An improved DTC-SVM method for matrix converter drives using a deadbeat scheme," *International Journal of Electronics*, Vol. 93, no. 11, pp. 737-753, Nov. 2006.

[9] K, -B. Lee and F. Blaabjerg, "Improved Direct Torque Control for Sensorless Matrix Converter Drives with Constant Switching Frequency and Torque Ripple Reduction," *International Journal of Control, Automation, and Systems*, Vol. 4, no. 1, pp. 113-123, Feb. 2006.

[10] R. Datta and V. T. Ranganathan, "Direct Power Control of Grid-Connected Wound Rotor Induction Machine without Rotor Position Sensors," *IEEE Transactions on Power Electronics*, Vol. 16, No. 3, pp. 390-399, May 2001.

[11] M. Malinowski, M. P. Kazmierkowski, S. Hansen, F. Blaabjerg, and G. D. Marques, "Virtual-flux-based direct power control of three-phase PWM rectifiers," *IEEE Transactions on Industry Applications*, Vol. 37, no. 4 pp. 1019-1027, Jul./Aug. 2001.

[12] A. Tapia, G. Tapia, J. X. Ostolaza, and Jose Ramon Saenz, "Modeling and Control of a Wind Turbine Driven Doubly Fed Induction Generator," *IEEE Transactions on Energy Conversion*, Vol. 18, no. 2, pp. 194-204, June 2003.

[13] Y. Lei, A. Mullane, G. Lightbody, and R. Yacamini, "Modeling of the Wind Turbine with a Doubly Fed Induction Generator for Grid Integration Studies," *IEEE Transactions on Energy Conversion*, Vol. 21, no. 1, pp. 257-264, Mar. 2006.

[14] G. Tapia, A. Tapia, J. X. Ostolaza, "Two Alternative Modeling Approach for the Evaluation of Wind Farm Active and Reactive Power Performances," *IEEE Transactions on Energy Conversion*, Vol. 21, no. 4, pp. 909-920, Dec. 2006.

[15] L. Mihet-Popa, F. Blaabjerg and I. Boldea, "Wind Turbine Generator Modeling and Simulation Where Rotational Speed is the Controlled Variable," *IEEE Transactions on Industry Applications*, Vol. 40, no. 1, pp. 3-10, Jan/Feb. 2004.

[16] B. Shen, B. Mwinyiwiwa, Y. Zhang, and B. –T. Ooi, "Sensorless Maximum Power Point Tracking of Wind by DFIG Using Rotor Position Phase Lock Loop (PLL)," *IEEE Transactions on Power Electronics*, Vol. 24, no. 4, pp. 942 – 951, Apr. 2009.

Sung-Tak Jou was born in Seoul, Korea, in 1979. He received the B.S. degree in Electronic Engineering from the Ajou University, Suwon, Korea, in 2005. He is currently working toward the M.S. degree at Ajou University. His research interests are power conversion and electric machine drives.

Sol-Bin Lee was born in Jeonju, Korea, in 1985. He received the B.S. degree in Electrical Engineering from Chonbuk National University, Jeonju, Korea, in 2008. He is currently working toward the M.S. degree at Ajou University. His research interests are grid-connected system and electric machine drives.

Yong-Bae Park was born in Daegu, Korea, in 1977. He received the B.S. (summa cum laude), M.S., and Ph.D. degrees in electrical engineering from the Korea Advanced Institute of Science and Technology, Daejeon, in 1998, 2000, and 2003, respectively. From 2003 to 2006, he was with the Korea Telecom Laboratory, Seoul, Korea. In 2006, he joined the School of Electrical and Computer Engineering, Ajou University, where he is now an assistant professor. His research interests include electromagnetic field analysis and electromagnetic interference and compatibility related to power electronics.

Kyo-Beum Lee was born in Seoul, Korea, in 1972. He received the B.S. and M.S. degrees in electrical and electronic engineering from the Ajou University, Korea, in 1997 and 1999, respectively. He received the Ph.D. degree in electrical engineering from the Korea University, Korea in 2003. From 2003 to 2006, he was

with the Institute of Energy Technology, Aalborg University, Aalborg, Denmark. From 2006 to 2007, he was with the Division of Electronics and Information Engineering, Chonbuk National University, Jeonju, Korea. In 2007 he joined the Division of Electrical and Computer Engineering, Ajou University, Suwon, Korea. He is an associate editor of the IEEE Transactions on Power Electronics and the Journal of Power Electronics. He has received two IEEE prize paper awards. His research interests include electric machine drives and wind power generations.